Exact time-dependent similarity solutions for isothermal shallow ice sheets

Ed Bueler, Craig S. Lingle, Jed A. Kallen-Brown, Latrice N. Bowman, and David N. Covey

ABSTRACT. We present a new family of *exact, time-dependent*, radially-symmetric "similarity" solutions to the isothermal shallow ice equation. We also present the one-horizontal dimension analog. (A similarity solution is one which depends on time and space through rescaling of a function of one variable.)

In the case of zero accumulation, the solution is analogous to the time-dependent "Green's function" of the heat equation. For instance, the solution becomes an arbitrarily tall column of ice localized in an arbitrarily small area as time $t \to 0^+$. As $t \to +\infty$ the solution becomes arbitrarily flat and widespread. The total ice volume is constant in time. If n is the Glen flow law exponent then the margin is at radius proportional to $t^{1/(5n+3)}$ and the central height is proportional to $t^{-2/(5n+3)}$. The zero accumulation solution, just described, is embedded in a one-parameter family of solutions with particular time-dependent accumulation or ablation profiles.

We use the simplest case among these exact solutions to evaluate and validate several one-horizontal dimension finite difference methods, namely explicit, semi-implicit and Crank-Nicolson. We also validate the explicit type I method against the radial exact solution. The methods are each shown to accurately track the location of the moving margin despite making their largest errors in the vicinity of that margin.

Introduction

The *isothermal, cold, shallow ice equation* is a single partial differential equation (PDE) for the thickness $h = h(t, x, y)$ of an ice sheet. It is derived in standard texts (Fowler 1997, Hutter 1983, Paterson 1994, van der Veen 1999). In summary, one supposes that

- the ice sheet has a single (solid) phase;

This manuscript, in exactly this form, was submitted electronically on 2 December, 2003 to *J. Glaciol.* The referees, two anonymous plus Richard Hindmarsh, pointed out the existence of four papers we did not know about, namely (Halfar 1981, Halfar 1983, Hindmarsh 1990, Nye 2000). Roland Warner also found these references. Halfar (1981) discovered the one horizontal dimension and zero accumulation solution below, and (Halfar 1983) addresses the radial version. The nonzero accumulation case ($\epsilon \neq 0$) below is new to our knowledge. A comparison of a numerical model to the similarity solution has not been published, to our knowledge. (ELB 2/11/04).

- solid ice is a slow moving, non-Newtonian fluid satisfying the Glen-Nye (Glen 1955, Nye 1957) constitutive relation (flow law) $\dot\epsilon_{ij} = A\,(\sigma')^{n-1}\sigma'_{ij}$ where $\dot\epsilon_{ij}$ is the strain rate tensor, $\sigma'_{ij} = \sigma_{ij} - \frac{1}{3}\delta_{ij}\sigma_{kk}$ is the deviatoric stress tensor, $\sigma' = \left(\sigma'_{ij}\sigma'_{ij}\right)^{1/2}$ is the effective shear stress, n is experimentally (Goldsby & Kohlstedt 2001) believed to be in the range $1.8 \le n \le 4$, and A is material parameter;[1]
- the ice sheet is shallow, allowing one to exclude shear stresses except in horizontal planes and compute the effective shear stress from the product of depth and surface slope (Fowler 1997, Hutter 1983);
- the ice sheet, in this case, is at a constant temperature.

In this paper we also suppose that the ice sheet rests on a rigid, flat bed at height zero and is frozen to this bed. In particular there is no distinction in this paper between height and thickness; both are "h".

The result of these assumptions is the equation

$$\frac{\partial h}{\partial t} = a + \nabla\cdot\left(\tfrac{\Gamma}{n+2}\,h^{n+2}|\nabla h|^{n-1}\nabla h,\right) \tag{1}$$

for the thickness $h = h(t,x,y)$ of the ice sheet. Here $a = a(t,x,y)$ is an ice-equivalent accumulation rate and $\Gamma = 2(\rho g)^n A > 0$ is constant. Also "$\nabla\cdot$" is the divergence and "∇" the gradient in the (horizontal) variables x, y.

The boundary condition applicable to (1) is that $h \ge 0$. In fact, the PDE (1) is more properly recast in (weak) variational inequality form, in which case the initial/boundary value problem has recently been proven to be well-posed (Calvo, Díaz, Durany, Schiavi & Vázquez 2002). In practice, there are various mechanisms to allow a numerical method to either fix the location of the margin or allow it to move (van der Veen 1999). In the results section we will validate one simple method for margin movement.

In this paper we derive the first time-dependent exact solution, to our knowledge, of (1). The two horizontal dimension version of this solution is radial $h = h(t,r)$. In the simplest case of zero accumulation it precisely conserves ice volume while the margin advances radially and the central peak decays. The solution is furthermore analogous to the time-dependent Green's function of the classical heat/diffusion equation in that it has "similarity" form and a delta function limit as $t \to 0^+$, as explained in the next section.

Following the derivation of this exact solution and its one horizontal dimension analog, and some comments on their interpretation, we use the one-horizontal-dimension similarity solution to compare the quality of several standard numerical schemes. We also validate the explicit type I (Hindmarsh & Payne 1996, Huybrechts et al. 1996) method in two horizontal dimensions using the radial solution.

We do not suppose that equation (1), much less the solution presented in this paper, is a sufficient model for ice sheets. Rather, we believe that by using this time-dependent solution the ice sheet modelling community can reduce its dependence on intercomparison in the isothermal case (Huybrechts et al. 1996). That is, exact time-dependent solutions

[1]Note that the strong dependence of A on temperature motivates generalizing (1) to a (thermo)coupled pair of evolution PDEs. Nonetheless, we address the isothermal case in this paper. Similarity solutions may exist in the thermocoupled case but their derivation is evidently much harder.

can and should be used for numerical validation, if possible. The addition of time-dependent solutions notably improves the previous situation which depended exclusively on exact steady state solutions and intercomparison of numerical models.

In a forthcoming paper (Bueler, Kallen-Brown, Lingle & Covey 2004) we will describe an analytical time-dependent solution to the *thermocoupled* shallow ice approximation. That solution is not as natural as the similarity solution of the current paper. However, it has been used for validation of a thermocoupled model; such use should further reduce dependence on model validation through intercomparison (Payne et al. 2000).

Method of similarity solutions

For understanding the computations in this section the reader should recall, for comparison, the time-dependent *Green's function*, or *fundamental solution*, of the linear heat (diffusion) equation. The equation is $\partial u/\partial t = \nabla \cdot (k \nabla u)$ where u represents a diffusive quantity such as temperature. Suppose $k > 0$ constant and consider two spatial dimensions.

The Green's function is then $\tilde{u}(t,x,y) = (4\pi k t)^{-1} e^{-(x^2+y^2)/4kt}$. Recall the properties of $\tilde{u}$. It satisfies $\lim_{t\to 0} \tilde{u}(t,x,y) = \delta(x,y)$ where δ is the Dirac delta (generalized) function. The solution $\tilde{u}$ therefore corresponds to starting with a unit amount of heat concentrated at the origin of the plane at time $t = 0$. The temperature diffuses as time goes on such that the total heat $\iint \tilde{u}(t,x,y)\,dx\,dy = 1$ for all time. Furthermore, $u(t,x,y) = \iint \tilde{u}(t,x-p,y-q) f(p,q)\,dp\,dq$ solves the heat equation with initial value $u(0,x,y) = f(x,y)$ (Evans 1998). That is, general solutions are built by convolution with this Green's function.

Now, $\tilde{u}$ is really a simple Gaussian function with a rescaling of time and space which turns out to make a time-dependent solution. That is, if $r^2 = x^2 + y^2$ then

$$\tilde{u}(t,r) = \frac{1}{t}\tilde{v}\left(\frac{r}{t^{1/2}}\right), \quad \text{where } \tilde{v}(q) = (4\pi)^{-1} e^{-q^2/4k}.$$

A solution of this type, which is a function of one variable scaled in a precise manner to become a time-dependent solution, is called a *similarity solution* (Evans 1998).

Though the shallow ice equation (1) *is nonlinear, it turns out we may still calculate such a "similarity" solution.* We are motivated by the Green's function of the heat equation above, of course, but we are also motivated by a similarity solution to the porous medium equation $\partial u/\partial t = \nabla \cdot (\nabla(u^\gamma))$, $\gamma > 1$, called *Barenblatt's* solution (Evans 1998). A similarity solution to the $\gamma = 2$ case of the porous medium equation appears in (Fowler 1997), section 5.1. In any case, we will find a solution to (1) with "Dirac delta initial data", which has such a similarity form, for particular accumulation profiles.

One may argue whether our solution is as "fundamental" to ice sheets as the Green's function above is "fundamental" to the heat equation. In fact, because the shallow ice equation is nonlinear, the similarity solution will *not* be directly useful in the construction of solutions to the ice equation for general initial data. The convolution technique mentioned for the heat equation clearly depends on the linearity of that equation. However, in light of the importance of Green's functions generally, this similarity solution of

the isothermal shallow ice equations may well be conceptually the most important exact time-dependent solution, if others are found.

In any case, for the isothermal shallow ice equation we seek a "similarity" solution of the form

$$h(t,x,y) = \frac{1}{t^\alpha} v\left(\frac{r}{t^\beta}\right) = t^{-\alpha} v(t^{-\beta} r). \tag{2}$$

Consider first the case of zero accumulation. Let $q = t^{-\beta} r$. Substitution of (2) into the $a \equiv 0$, isothermal shallow ice equation

$$\frac{\partial h}{\partial t} = \nabla \cdot \left(\tfrac{\Gamma}{n+2} h^{n+2} |\nabla h|^{n-1} \nabla h \right), \tag{3}$$

noting $\nabla f(q) = t^{-\beta} f'(q) \hat{\mathbf{r}}$ and $\nabla \cdot (f(q)\hat{\mathbf{r}}) = \frac{1}{r} \frac{d}{dr} (r f(q)) = t^{-\beta} \frac{1}{q} \frac{d}{dq} (q f(q))$, gives

$$-\alpha t^{-(\alpha+1)} v - \beta t^{-(\alpha+1)} q v' = \tfrac{\Gamma}{n+2} t^{-(2n+2)\alpha-(n+1)\beta} \tfrac{1}{q} \left(q v^{n+2} |v'|^{n-1} v' \right)' \tag{4}$$

where $v = v(q)$ and $v' = \frac{dv}{dq}$. Now, equation (4) becomes t–independent if the powers of t balance, so we suppose

$$\alpha + 1 = (2n+2)\alpha + (n+1)\beta. \tag{5}$$

We obtain an ordinary differential equation

$$\alpha v + \beta q v' + \tfrac{\Gamma}{n+2} \tfrac{1}{q} \left(q v^{n+2} |v'|^{n-1} v' \right)' = 0. \tag{6}$$

We construct $v = v(q)$ by solving equation (6), as follows. Multiplying through by q and also supposing

$$\alpha = 2\beta, \tag{7}$$

we recognize derivatives, $\frac{d}{dq} (\beta q^2 v) + \frac{\Gamma}{n+2} \frac{d}{dq} (q v^{n+2} |v'|^{n-1} v') = 0$, and thus for constant C,

$$\beta q^2 v + \tfrac{\Gamma}{n+2} q v^{n+2} |v'|^{n-1} v' = C. \tag{8}$$

Now, if $\lim_{q\to 0} v$ and $\lim_{q\to 0} v'$ are finite, and this we may verify of the formula which results, then we see $C = 0$ by taking the limit of both sides of equation (8). We may also verify $v'(q) \le 0$ for $q \ge 0$. We simplify (8) to get

$$\beta q = \tfrac{\Gamma}{n+2} v^{n+1} (-v')^n. \tag{9}$$

Taking the nth root and integrating from 0 to q gives

$$\left(\frac{\beta(n+2)}{\Gamma} \right)^{1/n} \frac{q^{1+1/n}}{1+1/n} = \frac{v_0^{2+1/n} - v(q)^{2+1/n}}{2+1/n}.$$

This simplifies to give the desired formula for v,

$$v(q) = \left[v_0^{2+1/n} - \Lambda q^{1+1/n} \right]^{n/(2n+1)} \tag{10}$$

where $\Lambda = \beta^{1/n} (n+2)^{1/n} \Gamma^{-1/n} (2n+1)(n+1)^{-1}$.

We have made two assumptions about the powers α and β in the assumed form $h = t^{-\alpha} v(t^{-\beta} r)$, namely equations (5) and (7). The solution is $\beta = (5n+3)^{-1}$ and

$\alpha = 2(5n+3)^{-1}$. With these constants, (10) gives us our goal, a similarity solution $h(t,r) = t^{-\alpha} v(t^{-\beta} r)$.

Theoretical Results

The calculation of the previous section has the following conclusion:

RESULT 1. *Suppose $n \geq 1$ and $\Gamma > 0$ are constants. Assume h_1 is a positive constant; it corresponds to the central height at $t = 1$.*[2] *Let*

$$\alpha = \frac{2}{5n+3}, \qquad \beta = \frac{1}{5n+3},$$

and let

$$\Lambda = \left(\frac{(n+2)\beta}{\Gamma}\right)^{1/n} \frac{2n+1}{n+1}, \qquad \Theta = h_1^{(2n+1)/(n+1)} \Lambda^{-n/(n+1)}.$$

For $t > 0$ and $(x,y) \in \mathbf{R}^2$ let

$$h(t,x,y) = h(t,r) = \begin{cases} t^{-\alpha} \left[h_1^{(2n+1)/n} - \Lambda \left(t^{-\beta} r\right)^{(n+1)/n} \right]^{n/(2n+1)}, & r < \Theta t^\beta, \\ 0, & r \geq \Theta t^\beta. \end{cases} \tag{11}$$

The function $h(t,x,y)$ is continuous for $t > 0$ and $(x,y) \in \mathbf{R}^2$. On the set $0 < r < \Theta t^\beta$ where $h > 0$, h is a smooth function of r. Furthermore, for $r < \Theta t^\beta$, h solves the partial differential equation (3).

It can be shown by substitution that the nonzero part of formula (11) is a solution to the $a \equiv 0$ case of the isothermal shallow ice equation (1), that is, to (3).

See figures 1 and 2. Note that the time-dependent margin of the ice is the expanding circle $r = \Theta t^\beta$. Also $h(t,0) = t^{-\alpha} h_1$ and thus $h_1 = h(1,0)$. We regard h_1 as the primary normalization parameter. There is no meaningful way to normalize "at $t = 0$" as the solution does not exist at that time. In fact, at $t = 0$, $h(t,x,y)$ is a Dirac delta (generalized) function. Reporting this fact is not particularly helpful, however, because the solution (11) cannot be used to construct general solutions, by convolution, to the nonlinear PDE (3), as in the analogous linear heat equation situation. Furthermore, though h is well-defined for $0 < t \ll 1$, and though h solves equation (3) for such times, the extreme height and small margin radius of h at such times (not shown) is incompatible with the shallow approximation which produced equation (3). We therefore regard h as a nonphysical abstraction for $0 < t \ll 1$, though an exact solution to the PDE (3).

Consider the significance of the radial solution (11). First, the solution has no steady state, and in fact the radius of the sheet goes to infinity as $t \to \infty$. Specifically, we have the new result that *the margin is at radius proportional to $t^\beta = t^{1/(5n+3)}$*, or $\sqrt[18]{t}$ if $n = 3$, in the radially-symmetric case. This might be regarded as a "natural" rate of margin

[2]This normalization depends on the choice of units of time. As addressed below, normalizing "at $t = 0$" would be meaningless, thus we choose central height at a particular time. In practice, $t = 1$ *year*.

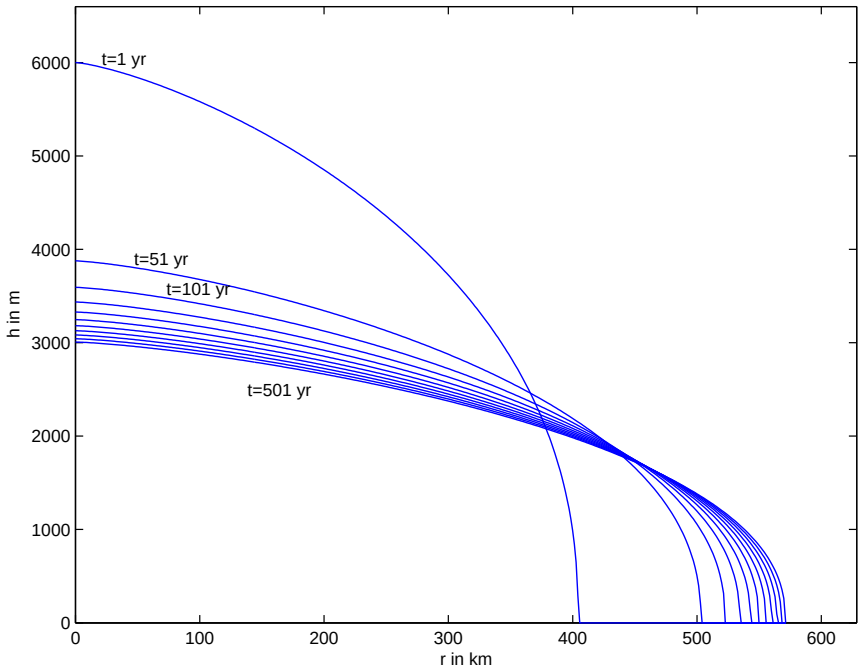

FIGURE 1. Radially-symmetric solution (11) of the zero accumulation isothermal shallow ice equation (3) for $t = 1$ year and at 50 year intervals thereafter. Here $n = 3$, $\Gamma = 2(\rho g)^3 A$, $\rho = 910\text{kg/m}^3$, $A = 10^{-16}\,1/(\text{Pa}^3\text{yr})$, and $h_1 = 6000\text{m}$.

movement as it is not driven by accumulation or retarded by ablation. (For the one-horizontal-dimension case below, the margin is at radius proportional to $t^\gamma = t^{1/(3n+2)}$, or $\sqrt[11]{t}$ if $n = 3$. That is, the radius advances more rapidly in one dimension as expected.)

The central peak decays at a particular time-dependent rate. Namely, for solution (11) the height of the center is proportional to $t^{-\alpha} = t^{-2/(5n+3)}$, or $\frac{1}{\sqrt[9]{t}}$ if $n = 3$. (For one horizontal dimension, below, the divide height is proportional to $t^{-\gamma} = t^{-1/(3n+2)}$, or $\frac{1}{\sqrt[11]{t}}$ if $n = 3$.)

Consider the shape of the margin. Fix $t > 0$ and let $L = \Theta t^\beta$ be the position of the margin (i.e. the margin is at $r = L$). In equation (11) the expression $\phi(r) = h_1^{(2n+1)/n} - \Lambda(rt^{-\beta})^{(n+1)/n}$ is zero at $r = L$ and has finite derivative $\phi'(L) < 0$ at $r = L$. Thus[3] $\phi(r) \sim L - r$ as $r \to L^-$. It follows that

$$h(t, r) \sim (L - r)^{n/(2n+1)} \tag{12}$$

as $r \to L^-$, where L is the (time-dependent) location of the margin.

The asymptotic expression (12) is of some interest relative to known margin shapes. Such shapes are classically known in the isothermal steady state cases of margin-in-accumulation-zone and margin-in-ablation-zone (Fowler 1997, Paterson 1994). It turns

[3]By definition, $f(x) \sim g(x)$ as $x \to a$ if $f(x)/g(x) \to C > 0$ as $x \to a$.

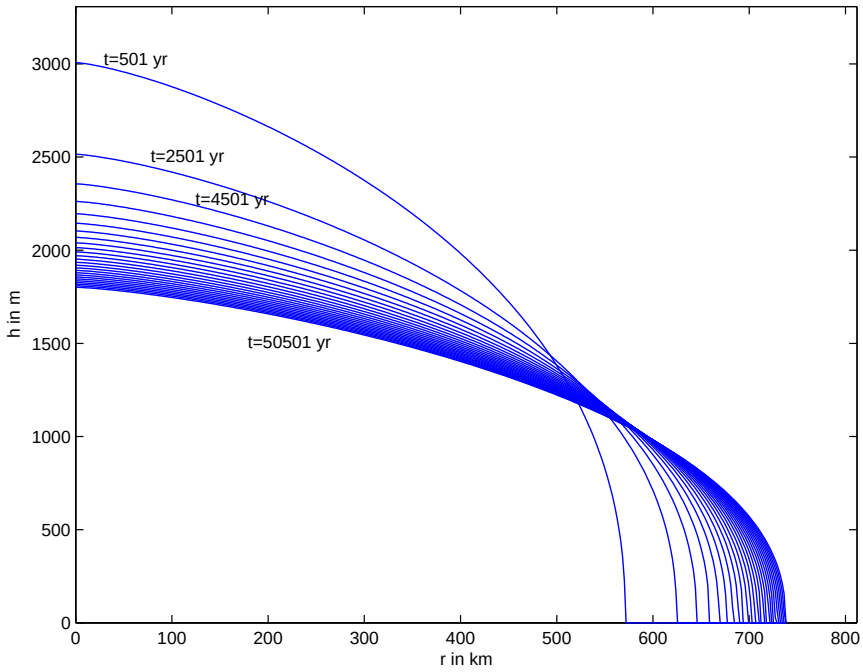

FIGURE 2. Solution (11) with the same constants as above, but displayed for $t = 501$ years and at 2000 year intervals thereafter. Note dramatic slowing of margin advance; the margin is at position $r \sim \sqrt[18]{t}$.

steady state	time-dependent	steady state
$a > 0$ (accumulation)	$a \equiv 0$	$a < 0$ (ablation)
$h \sim (L-r)^{n/(2n+2)}$	$h \sim (L-r)^{n/(2n+1)}$	$h \sim (L-r)^{n/(2n+0)}$

TABLE 1. Comparison of asymptotic margin shapes.

out that the asymptotic margin shape for this time-dependent but zero accumulation solution is intermediate between the accumulation and ablation steady state cases, as shown in table 1.

It follows from (12) that the radial solution (11) has arbitrarily large basal (effective) shear as $r \to L$. This singularity for stress applies to accumulation-zone steady state margins as well but contrasts with ablation-zone steady margins where the basal stress remains finite as $r \to L$.

The total volume of ice $V(t) = \iint h(t,x,y)\,dx\,dy$ is constant for all $t > 0$. In the radial case clearly $V(t) = 2\pi \int_0^{\Theta t^\beta} rh(t,r)\,dr$. The change of variable $r = qt^\beta$ gives

$$V(t) = 2\pi \int_0^\Theta q \left[h_1^{(2n+1)/n} - \Lambda q^{(n+1)/n}\right]^{n/(2n+1)} dq = V(1). \tag{13}$$

Note $t^\alpha = (t^\beta)^2$. The volume is therefore independent of time, as expected from the mass balance $a \equiv 0$. (The actual evaluation of $V(1)$ involves a difficult integral in general, though the $n = 1$ case is easy. Other cases can be evaluated numerically.)

We now state the one horizontal dimension analog of the above radial solution.

RESULT 2. *Following roughly the argument that led to* (11)*, we derive a similarity solution to the equation*

$$\frac{\partial h}{\partial t} = \frac{\partial}{\partial x}\Big(\frac{\Gamma}{n+2} h^{n+2} \left|\frac{\partial h}{\partial x}\right|^{n-1} \frac{\partial h}{\partial x}\Big),$$

that is, to the isothermal shallow ice equation in one horizontal dimension with $a \equiv 0$. In particular, for $\gamma = (3n+2)^{-1}$ the solution is

$$h(t,x) = t^{-\gamma}\left[h_1^{(2n+1)/n} - \tilde\Lambda\left(t^{-\gamma}|x|\right)^{(n+1)/n}\right]^{n/(2n+1)}, \tag{14}$$

where $\tilde\Lambda = \left(\frac{(n+2)\gamma}{\Gamma}\right)^{1/n} \frac{2n+1}{n+1}$ and $\tilde\Theta = h_1^{(2n+1)/(n+1)} \tilde\Lambda^{-n/(n+1)}$. This formula applies for $|x| < \tilde\Theta t^\gamma$; outside of this time-dependent interval the solution is zero.

Again the result can be verified by substitution. This one-horizontal dimension solution can be regarded, if desired, as a two dimensional solution, namely, an infinitely long or periodic ridge of ice with y-independent cross-section.

Family of solutions with nonzero accumulation/ablation. Inspection of the above derivation suggests a modest generalization. The result is a one-parameter ("ϵ" below) family of similarity solutions. When $\epsilon = 0$ we recover the solution already described. For $\frac{-1}{2n+1} < \epsilon < 0$ the solutions correspond to ablation everywhere on the ice sheet, in a spatially-dependent and decaying-in-time amount. For $\epsilon > 0$ the solutions correspond to accumulation everywhere. When ϵ reaches the critical value $\bar\epsilon = \frac{2}{n+1}$, the magnitude of the accumulation is sufficient to cause the maximum height of the ice sheet to grow in time.

RESULT 3. *Suppose $n \geq 1$ and $\Gamma > 0$ are constants. Assume h_1 is a positive constant—it corresponds to the central height at $t = 1$. Let ϵ be a real parameter in the range*

$$\frac{-1}{2n+1} < \epsilon < +\infty.$$

Let

$$\alpha(\epsilon) = \frac{2-(n+1)\epsilon}{5n+3}, \qquad \beta(\epsilon) = \frac{1+(2n+1)\epsilon}{5n+3}. \tag{15}$$

Note $\beta(\epsilon) > 0$ for allowed ϵ while $\alpha(\epsilon)$ changes sign at $\bar\epsilon = \frac{2}{n+1}$. Let

$$\Lambda(\epsilon) = \left(\frac{(n+2)\beta(\epsilon)}{\Gamma}\right)^{1/n} \frac{2n+1}{n+1}, \qquad \Theta(\epsilon) = h_1^{(2n+1)/(n+1)} \Lambda(\epsilon)^{-n/(n+1)}.$$

Let

$$v_\epsilon(q) = \left[h_1^{(2n+1)/n} - \Lambda(\epsilon) q^{(n+1)/n}\right]^{n/(2n+1)}.$$

For $t > 0$ and $r \geq 0$ let

$$h^{(\epsilon)}(t,r) = \begin{cases} t^{-\alpha(\epsilon)}\, v_\epsilon\left(t^{-\beta(\epsilon)} r\right), & r < \Theta(\epsilon) t^{\beta(\epsilon)}, \\ 0, & r \geq \Theta(\epsilon) t^{\beta(\epsilon)}. \end{cases}$$

and let

$$a^{(\epsilon)}(t,r) = \epsilon\, t^{-1}\, h^{(\epsilon)}(t,r).$$

The functions $a^{(\epsilon)}(t,r)$ and $h^{(\epsilon)}(t,r)$ are continuous for $t > 0$ and $r \geq 0$. On the set $0 < r < \Theta(\epsilon) t^{\beta(\epsilon)}$ they are smooth functions of r. Furthermore, for $r < \Theta(\epsilon) t^{\beta(\epsilon)}$, they solve the partial differential equation

$$\frac{\partial h^{(\epsilon)}}{\partial t} = a^{(\epsilon)} + \nabla \cdot \left(\tfrac{\Gamma}{n+2} \left(h^{(\epsilon)}\right)^{n+2} |\nabla h^{(\epsilon)}|^{n-1} \nabla h^{(\epsilon)} \right), \tag{16}$$

that is, the isothermal shallow ice equation with the particular accumulation profile $a^{(\epsilon)}$.

This family of solutions was derived by returning to equation (4) and noting that if the accumulation/ablation function a took the form $a = \epsilon\, t^{-(\alpha+1)} v$ then the same essential procedure which led to equation (9) would still work. However, one must alter α, β to make it so. In fact, equations (5) and (7) are replaced by the ϵ-dependent system

$$(2n+1)\alpha + (n+1)\beta = 1, \qquad -\alpha + 2\beta = \epsilon,$$

whence formulas (15).

Note that the function $a^{(\epsilon)}$ has the same sign as ϵ everywhere on the sheet and the same spatial shape as $h^{(\epsilon)}$ though because of the t^{-1} factor it "starts bigger" and "decays faster." Also, $a^{(\epsilon)}$ goes to zero at the edge of the sheet. The margin shape of the ice is indeed the *same* as described in the previous subsection; the margin is asymptotically in an "$a = 0$ zone."

Figure 3 shows the profile $h^{(\epsilon)}$ at a fixed time and for several values of ϵ.

Figure 4 shows total ice sheet volumes as functions of time for some values of ϵ. Numerical integration was not necessary to produce figure 4. In particular, the volume of the ice sheet determined by $h^{(\epsilon)}$ at time t is the integral

$$V(t,\epsilon) = 2\pi \int_0^{\Theta(\epsilon)\, t^{\beta(\epsilon)}} t^{-\alpha(\epsilon)} v_\epsilon\left(t^{-\beta(\epsilon)} r\right)\, r\, dr.$$

The substitutions $r = q t^{\beta(\epsilon)}$ and $s = \beta(\epsilon)^{1/(n+1)} q$, and the fact that $-\alpha(\epsilon) + 2\beta(\epsilon) = \epsilon$, produce the formula

$$V(t,\epsilon) = W_1 \beta(\epsilon)^{-2/(n+1)}\, t^\epsilon, \tag{17}$$

where

$$W_1 = 2\pi \int_0^{\hat{\Theta}} s \left[h_1^{(2n+1)/n} - \hat{\Lambda} s^{(n+1)/n} \right]^{n/(2n+1)} ds,$$

$\hat{\Lambda} = \left(\frac{n+2}{\Gamma}\right)^{1/n} \frac{2n+1}{n+1}$, and $\hat{\Theta} = h_1^{(2n+1)/(n+1)} \hat{\Lambda}^{-n/(n+1)}$. That is, the volume growth of the solution in result 3 is t^ϵ with an ϵ-dependent constant. In practice, numerical integration would likely be required to determine W_1 in terms of h_1, for instance.

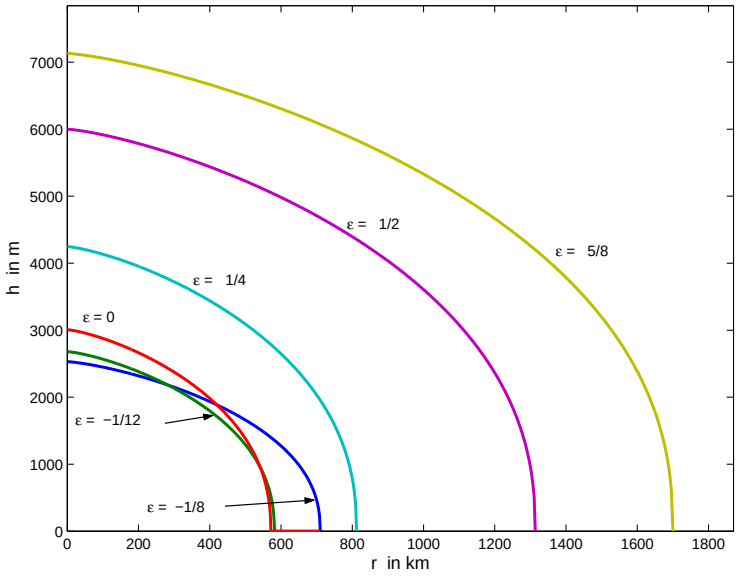

FIGURE 3. Profiles $h^{(\epsilon)}$ for $\epsilon = -1/8, -1/12, 0, 1/4, 1/2, 5/8$ at $t = 501$ years. Here $n = 3$, $\Gamma = 2(\rho g)^3 A$, $\rho = 910\text{kg/m}^3$, $A = 10^{-16}\, 1/(\text{Pa}^3\text{yr})$, and $h_1 = 6000\text{m}$. Note that for $\epsilon = \bar{\epsilon} = 1/2$ the central height at $t = 501$ years is the same as at $t = 1$ year.

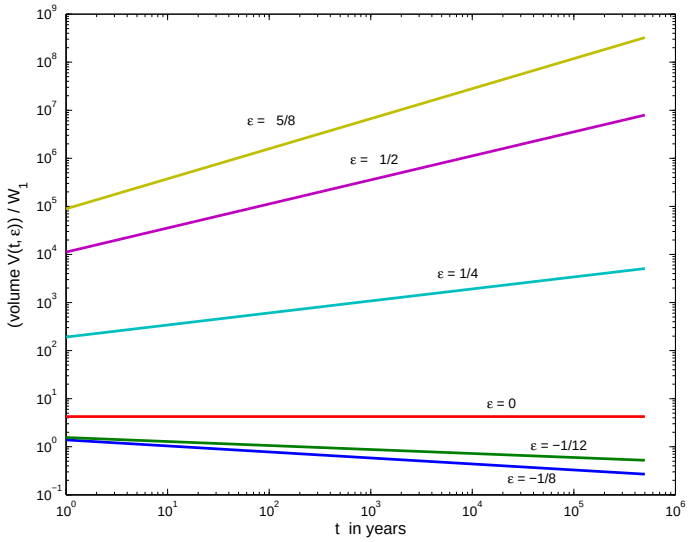

FIGURE 4. Total ice volume over time in units of W_1 for $\epsilon = -1/8, -1/12, 0, 1/4, 1/2, 5/8$. See equation (17). Same constants as in figure 3. Note logarithmic scales on both axes.

Application: Evaluation/Validation of finite difference numerical methods

In this section we use a time-dependent similarity solution to evaluate some of the standard finite difference methods. In summary, they work; they accurately reproduce

the time-dependent analytical solutions with errors varying somewhat between the chosen methods. Our tests represents the first validation of these methods in a time-dependent situation, to our knowledge. In particular, these methods show a clear ability to accurately "track" a moving margin over time, but they also show largest errors near the margin; this apparent paradox will be partly explained below.

We compare the explicit (Morton & Mayers 1994, van der Veen 1999), semi-implicit, and Crank-Nicolson (Mahaffy 1976, Morton & Mayers 1994) methods, along with a method which is explicit but uses a transformation introduced by (Calvo et al. 2002). This is done in one horizontal dimension for simplicity. A *Matlab* code implementing the following comparison is publicly available[4]. We consider the $a \equiv 0$ case; the equation for thickness $h(t,x)$ is

$$\frac{\partial h}{\partial t} = \frac{\partial}{\partial x}\Big(\frac{\Gamma}{n+2}h^{n+2}\left|\frac{\partial h}{\partial x}\right|^{n-1}\frac{\partial h}{\partial x}\Big). \tag{18}$$

Suppose a finite difference numerical method to approximate h on the time interval $[0,T]$ and spatial interval $[-L,L]$, with time steps $\Delta t = T/M$ and grid spacing $\Delta x = L/N$. Suppose $h_{l,j}$ approximates $h(l\Delta t, j\Delta x)$ for $l = 0,\dots,M$, $j = -N/2,\dots,N/2$.

There are two standard methods of approximating the vertically-averaged horizontal flux $Q = -\frac{\Gamma}{n+2}h^{n+2}\left|\frac{\partial h}{\partial x}\right|^{n-1}\frac{\partial h}{\partial x}$ at positions halfway between the spatial grid points (i.e. on the staggered grid). The *type I* method (Hindmarsh & Payne 1996, Huybrechts et al. 1996) approximates $Q(l\Delta t,(j+1/2)\Delta x)$ by

$$Q^{\rm I}_{j+1/2} = -D_{j+1/2}\frac{h_{j+1}-h_j}{\Delta x} \quad \text{where} \quad D_{j+1/2} = \frac{\Gamma}{n+2}\left(\frac{h_{j+1}+h_j}{2}\right)^{n+2}\left|\frac{h_{j+1}-h_j}{\Delta x}\right|^{n-1}$$

(Time indices l will be suppressed when the meaning is clear.) Alternately, the *type II* approximation of the same quantity is

$$Q^{\rm II}_{j+1/2} = -D^{\rm av}_{j+1/2}\frac{h_{j+1}-h_j}{\Delta x}$$

$$\text{where} \quad D^{\rm av}_{j+1/2} = \frac{D_{j+1}+D_j}{2} \text{ and } D_j = \frac{\Gamma}{n+2}h_j^{n+2}\left|\frac{h_{j+1}-h_{j-1}}{2\Delta x}\right|^{n-1}.$$

The quantities denoted by "D" are called *diffusivities* here.[5] We then form the standard approximation of the right side of equation (18) at a given time, namely $-\frac{\partial Q}{\partial x}\Big|_{x=j\Delta x} \approx -\frac{1}{\Delta x}\left(Q_{j+1/2}-Q_{j-1/2}\right)$.

There are at least three standard time-stepping strategies. The simplest is the *explicit method* (van der Veen 1999) wherein equation (18) is approximated by

$$\frac{h_{l+1,j}-h_{l,j}}{\Delta t} = -\frac{1}{\Delta x}\left(Q_{l,j+1/2}-Q_{l,j-1/2}\right). \tag{19}$$

[4]At `www.math.uaf.edu/~bueler/simice.m`.

[5]This language is motivated by considering a constant value D appearing in a heat/diffusion equation $\frac{\partial u}{\partial t} = \frac{\partial}{\partial x}\left(D\frac{\partial u}{\partial x}\right)$. In that case D would control the rate of diffusion. The word "*conductivity*" could also be applied to D, however, that might produce confusion in the context of thermocoupled ice models.

An alternative is to seek stability (though not greater accuracy[6]) through evaluating the diffusivities $D_{j+1/2}$ explicitly but the additional gradient factor in Q implicitly, so the method is *semi-implicit*:

$$\frac{h_{l+1,j} - h_{l,j}}{\Delta t} = \frac{1}{\Delta x}\left(D_{l,j+1/2}\frac{h_{l+1,j+1} - h_{l+1,j}}{\Delta x} - D_{l,j-1/2}\frac{h_{l+1,j} - h_{l+1,j-1}}{\Delta x}\right). \tag{20}$$

In the one horizontal dimension case a linear tridiagonal system must be solved at each stage; in two horizontal dimensions a standard technique for dealing with the resulting linear system is *Alternating Direction Implicit* (ADI) (Morton & Mayers 1994). Next, a more accurate discretization with good stability properties (for linear problems, at least (Morton & Mayers 1994)) is the Crank-Nicolson method

$$\frac{h_{l+1,j} - h_{l,j}}{\Delta t} = -\frac{1}{2\Delta x}\left(Q_{l+1,j+1/2} - Q_{l+1,j-1/2} + Q_{l,j+1/2} - Q_{l,j-1/2}\right). \tag{21}$$

Both left and right sides of equation (18) have been approximated by formulas symmetric around $(t_{l+1/2}, x_j) = ((l+1/2)\Delta t, j\Delta x)$, which is the source of accuracy. This method was introduced by Mahaffy (Mahaffy 1976) for the shallow ice equation. In a short appendix we comment on the implementation of this method.

In addition to the standard methods above, (Calvo et al. 2002) propose transforming equation (18) by $u = h^m$ for $m = (2n+2)/n$ (i.e. $u = h^{8/3}$ in the $n = 3$ case). Note $h^{n+2}\left|\frac{\partial h}{\partial x}\right|^{n-1}\frac{\partial h}{\partial x} = \omega_n\left|\frac{\partial u}{\partial x}\right|^{n-1}\frac{\partial u}{\partial x}$ by this transformation, where $\omega_n = (n/(2n+2))^n$. Equation (18) is therefore equivalent to

$$\frac{\partial}{\partial t}\left(u^{1/m}\right) = \frac{\partial}{\partial x}\Big(\frac{\omega_n\,\Gamma}{n+2}\left|\frac{\partial u}{\partial x}\right|^{n-1}\frac{\partial u}{\partial x}\Big). \tag{22}$$

When discretizing the right side of this equation we choose to approximate $\frac{\partial u}{\partial x}$ onto the stagger grid using values of u on the regular grid in the usual manner.[7] Clearly the explicit, semi-implicit, and Crank-Nicolson strategies could apply to (22); in what follows we use the explicit method for simplicity. The advantage of this technique is that the derivatives of the solution are finite, though still discontinuous, at the margin. A potential disadvantage is the transformation $u = h^m$ may not be implementable throughout a *thermocoupled* shallow ice model. In any case, there turns out not to be a significant advantage when the error is measured by comparing computed h values to the correct h values.

[6] "Accuracy" here means *local truncation error* (Morton & Mayers 1994). Explicit and semi-implicit methods have $O(\Delta t, \Delta x^2)$ local truncation error and Crank-Nicolson has $O(\Delta t^2, \Delta x^2)$ error *if* $h(t,x)$ *were smooth and its derivatives were finite*. This assumption fails at the margin. Thus it is *not* clear in theory what local, much less global, error is expected when modelling a moving margin by a finite difference or finite element method. Thus the need for validation with an exact time-dependent solution, now possible.

[7] That is, $\left.\frac{\partial u}{\partial x}\right|_{x=j\Delta x} \approx (u_{j+1/2} - u_{j-1/2})/\Delta x$. In some sense this is a type I choice. In fact the distinction between the types fades because only derivatives of u appear in the flux expression.

There are nine different schemes in the above analysis. Of these we test five, namely explicit type I, explicit type II, semi-implicit type I, Crank-Nicolson type I, and explicit-equation-(22).

A comment must be made on the numerical boundary condition. We claim, with support from the recent work of (Calvo et al. 2002), that the *correct* boundary condition for the isothermal shallow ice equation is the inequality constraint $h \geq 0$. The numerical boundary condition we impose is simply to maintain this constraint. That is, at each time step new values for h are computed. If any of those values are negative, we set such values to zero.[8] Also, in our tests we extend the grid sufficiently far so that a good numerical approximation will never have ice reach the edge of the grid.

In figure 5 we show the result of applying the explicit type I method. The initial value is the $t = 100$ year state of the similarity solution (14). We compute values of h at thirty points on a grid with $\Delta x = 97$ km. On the one hand we compute 30000 steps of the numerical method, with $\Delta t = 3.33$ years, to approximate the solution at $t = 100,000$ years. On the other hand we show as a solid curve the exact solution (14) at $t = 100,000$ years. There is clear agreement; figure 5 is a picture of success. Nonetheless there is error and we study it. Remarkably, the error actually decreases over time, as we shall explain.

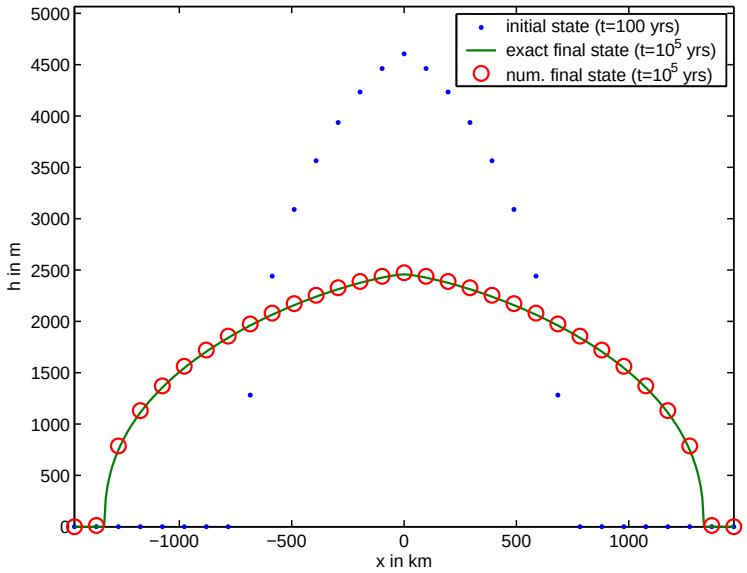

FIGURE 5. Result of explicit type I method compared to exact similarity solution. Here $n = 3$, $\Gamma = 2(\rho g)^3 A$, $\rho = 910\text{kg/m}^3$, $A = 10^{-16}\,1/(\text{Pa}^3\text{yr})$, and $h_1 = 7000$m. The small error in the vicinity of the margin is barely visible.

Figures 6 and 7 compare the error over time for the explicit type I and type II methods. Each point in these figures represents the maximum error over all spatial grid points at the given time. The maximum error made over time does not significantly distinquish

[8]See (Calvo et al. 2002) for a finite element method which systematically uses the constraint $h \geq 0$.

the two methods, though the shape of the error graph differs distinctly.[9] Note that in both graphs there is a cycle of increasing length. This variation of error is such that the largest errors in a cycle are roughly 20 times larger than the smallest.

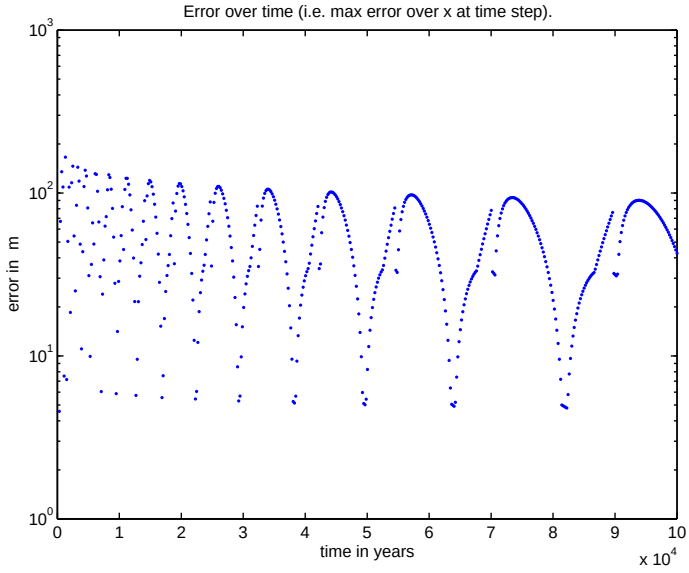

FIGURE 6. Error over time from explicit type I method. Numerical computation from $t = 100$ years to $t = 100,000$ years, with steps $\Delta t = 0.2$ years, 100 horizontal grid points, and grid spacing 29 km (finer than in figure 5), compared to exact similarity solution at successive times. Same physical constants as in figure 5.

Spatially, it turns out that these maximum errors always occur near the margin (not shown; compare figure 8 for the two horizontal dimension case). The cycling over time of the error comes from the movement of the exact margin position past successive grid points at a slowing rate. In fact, the essential source of error is not the accumulation of (local truncation) error over time but simply the failure of a piecewise linear approximation to closely model the "(3/7)th root" (for $n = 3$) margin shape. Note that finite difference *and* finite element methods, including in 3D, will always experience such error, and the use of (e.g.) quadratic finite elements does not improve the situation.

The slowly decreasing error magnitude is a consequence of the gradual thinning of the sheet. All of the methods are successful at not growing the (accumulating local truncation) error so as to "swamp" the effect of a thinner sheet. In some sense, perhaps, the time-stepping method sees a "quasi-steady-state" while still moving the margin at the correct rate.

Table 2 below summarizes a systematic comparison of the five methods we have tested. The comparison is between the similarity solution at each numerical time step and the

[9]The shape seems to go with type and not the time-stepping method, as, for instance, the semiimplicit and Crank-Nicolson type I error graphs are similar to the explicit type I error graph.

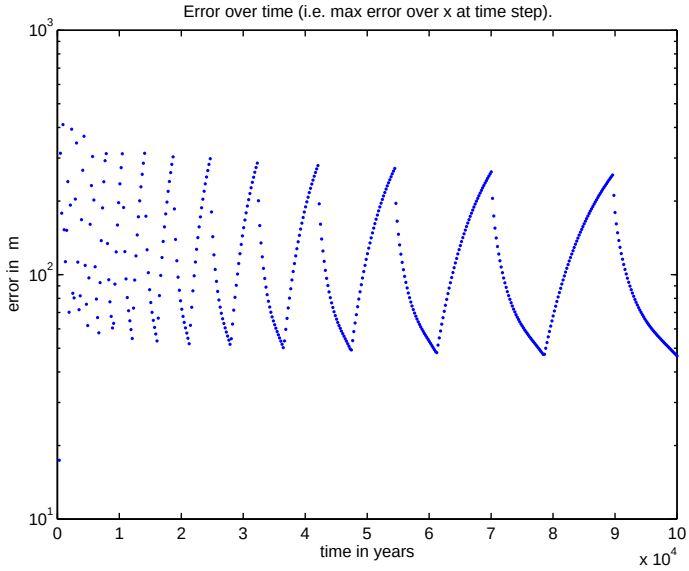

FIGURE 7. Error over time from explicit type II method. Same numerical parameters and constants as in figure 6 except that $\Delta t = 0.6$ years (as type II is somewhat more stable).

Method	N	Maximum apparently stable Δt [a]	Δt chosen [a]	Exec. time [s]	Max. error over time [m]	Max. error at last time [m]
explicit type I	30	12	6	8	381	41
same	100	0.40	0.20	365	232	41
explicit type II	30	46	23	2	803	162
same	100	1.2	0.60	127	510	46
semi-implicit type I	30	1800	900	0.2	1651	24
same	100	25	12	18	386	45
Crank-Nicolson type I	30	210	105	33	698	41
same	100	25	12	985	397	41
explicit w. $u = h^{8/3}$	30	13	6	8	472	54
same	100	0.40	0.20	472	295	13

TABLE 2. Comparison of five numerical methods versus the similarity solution (14), computing from $t = 100$ year state as initial condition till $t = 100,000$ year state. Same physical constants as in figure 5.

numerical state at that time, in a computation from $t = 100$ years to $t = 100,000$ years, with physical constants as in figure 5.

In order to realistically compare the methods, and instead of using a fixed time step for all methods, we attempted to find the maximum stable time step and then use half of that value in the computation. Note that for all of the methods and for both $N = 30$ and $N = 100$, sufficiently big time steps make the computation either explode (typical of

explicit methods) or enter a peculiar and completely nonphysical limit cycle (Hindmarsh & Payne 1996) (for semi-implicit and Crank-Nicolson methods). This limit cycle is most easily detected by observing the diffusivity D; the surface elevation may be only very slightly modified by a huge sawtooth instability in the diffusivity D. Instabilities first appear where D is greatest, as noted.

The execution time of a *Matlab* program on a Pentium III (800 MHz, 256 Kb cache memory, 128 Mb memory) desktop machine is reported. At the time of preparation of this article this machine was already regarded as very modest in speed for a desktop computer. In any case, these execution times are for preliminary comparison among the methods only; no serious attempt was made at optimizing the methods.

A maximum error which is the absolute value of the difference between the exact and numerical solutions over all spatial grid points is computed at each time. Only the maximum value of this maximum error over time, and the last value of this maximum error, are reported. The values of the error should be compared to the central height of the sheet relevant to the computation, that is, to the central height at $t = 100$ years, which is 4606 m. (The maximum extent of the sheet was $L = 1334$ km at the last time, namely $t = 100,000$ years.) There is rough agreement in maximum error over time for all these methods. It turns out (see figures 6 and 7) that the maximum error over time occurs at early stages when the ice sheet is thickest. By contrast to the maximum error over time, the error at the last time is substantially a matter of "luck" in sampling the error cycle depicted in figures 6 and 7 and is therefore of little significance. We recommend that an average or maximum over many times should be reported, whenever possible, in a moving margin situation, for instance, in intercomparison.

Note that when the number of grid intervals is increased from $N = 30$ to $N = 100$ there is (generally) a reduction of maximum error over time by a factor of (roughly[10]) 0.6. This is definitely not explained by the $O(\Delta x^2)$ local truncation error one might compute for each of these methods if one assumed that spatial derivatives were bounded. Instead, note that $(30/100)^{3/7} = 0.597$. In fact, the reduction of maximum error is believed to be related to the modest improvement in a piecewise-linear approximation of the $(L-x)^{3/7}$ margin shape which one achieves by reducing the spatial grid size (in this case by a factor of 30/100).

Finally, we have validated the explicit type I method in two horizontal dimensions by comparing a numerical computation on a standard 2D horizontal grid to the radial solution (11). We used physical parameters $n = 3$, $\Gamma = 2(\rho g)^3 A$, $\rho = 910\text{kg/m}^3$, $A = 10^{-16}\,1/(\text{Pa}^3\text{yr})$, and $h_1 = 6000$ m. A 60 by 60 grid with $\Delta x = \Delta y = 35$ km spacing was used. We computed from $t = 101$ years to $t = 50101$ years with time steps of $\Delta t = 2/3$ year—this step was chosen to be within a factor of two of the longest stable time step. We used the $t = 101$ state of (11) as the initial condition and compared the final state to the $t = 50101$ state of the exact solution (11).

[10]The distinct exception to this generalization is in the semi-implicit method which allowed such long time steps in the $N = 30$ case that the early stages of a thick sheet may have been "bypassed" in some sense. Note the error in this case is quite large as a fraction of the $t = 100$ thickness of the sheet.

The main result of the calculation is to confirm that the most significant error appears near the margin where the thickness is changing rapidly as a function of the spatial variables. There is no need to display the final numerical state because it is so similar to the exact result shown in figure 2. Figure 8 shows the 1, 4, 16, and 64 m contours of the error computed as the absolute value of the difference between the exact and numerical solutions at time $t = 50101$ years. Error exceeding 16 m is confined to a close neighborhood of the margin. This neighborhood turns out to be roughly two grid spaces (i.e. 70 km) wide. The error is not radially symmetric; it shows the expected "grid effect".

The maximum error anywhere on the grid at the last time is 140 m. The maximum error over time is much larger and was not computed; computing the exact solution at each time would dominate the execution time of this explicit method. By stopping the computation at a sampling of earlier times, the maximum error over time is known to be at least 205m.

Figure 8 is a picture of success. Namely, we have used a simple numerical method to study a non-steady-state ice flow problem for which—this is a new situation!—an exact solution is known.

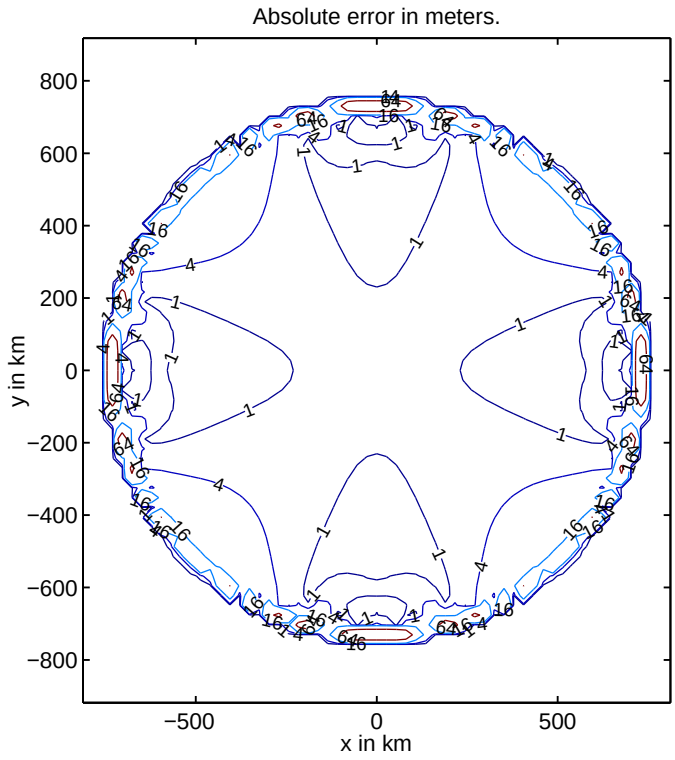

FIGURE 8. Error at last time from explicit type I method on a two horizontal dimension problem. See text for numerical parameters and physical constants.

Conclusion

Exact solutions play an important supporting role in numerical simulation of systems governed by nonlinear partial differential equations (e.g. in Newtonian fluids). This is already true of ice physics to a limited degree. However, until now exact solutions for shallow ice have been limited to steady solutions, sometimes supplemented by asymptotic and perturbation methods which incorporate time dependence (Fowler 1997). For instance, the basic EISMINT benchmarks (Huybrechts et al. 1996) include comparison to exact steady solutions. Though many simulations address ice sheet configurations believed to be close to steady state, the deviation from steady state is frequently the quantity of interest. A steady exact solution gives no direct information about the rate of deviation, though it can be used for a study based on linearization around the steady state, for instance. With the similarity solutions in this paper the situation may change. Ice sheet simulation programs which claim to address grounded moving margins can be compared, in an admittedly special isothermal case, to exact margin movement rates.

Furthermore, the similarity solutions in this paper show clearly the distinction between *stability* and *accuracy* of numerical methods for time dependent ice sheets. Instabilities in ice sheet simulations are to some degree localized where the diffusivity D is greatest (Hindmarsh & Payne 1996).[11] In particular, instabilities are localized away from peaks/ridges and margins. On the other hand, the results of this paper confirm rigorously that the inaccuracies in numerical approximation, those present even in a stable run, in the moving margin case, occur in the vicinity of margins.

Our comparison of an exact time-dependent solution to numerical results represents the first precise validation of numerical time-stepping schemes. Certain finite element methods are actually equivalent to the finite difference methods we consider, at least in one horizontal dimension. Indeed, our conclusions broadly apply to finite element methods because we have identified the difficulty in simulation of a moving margin as the difficulty of approximating a root (e.g., $h \sim (L-r)^{3/7}$ in the $n = 3$ case studied here) by piecewise linear (or in any case, polynomial) functions. Approximation by piecewise polynomial functions is at the foundation of finite difference/finite element methods.

We believe that the existence of exact, time-dependent solutions should reduce dependence in the ice modelling community on intercomparison as a validation method.

Acknowledgements

We thank the NASA Cryospheric Sciences Program for supporting this research with grant NAG5-11371, and Martin Truffer for his interest and comments on this work.

References

Bueler, E., Kallen-Brown, J. A., Lingle, C. S. & Covey, D. N. (2004), Time-dependent analytical solutions and numerical validation for thermocoupled shallow ice sheet models. In preparation.

[11] In the isothermal case with thickness H and surface elevation h, $D = \frac{\Gamma}{n+2} H^{n+2} |\nabla h|^{n-1}$ and $Q = -D\nabla h$ is the vertically-integrated horizontal flux.

Calvo, N., Díaz, J., Durany, J., Schiavi, E. & Vázquez, C. (2002), 'On a doubly nonlinear parabolic obstacle problem modelling ice sheet dynamics', *SIAM J. Appl. Math.* **63**(2), 683–707.
Evans, L. C. (1998), *Partial differential equations*, Vol. 19 of *Graduate Studies in Mathematics*, American Mathematical Society.
Fowler, A. C. (1997), *Mathematical Models in the Applied Sciences*, Cambridge Univ. Press.
Glen, J. W. (1955), 'The creep of polycrystalline ice', *Proc. Royal Soc. London A* **228**, 519–538.
Goldsby, D. L. & Kohlstedt, D. L. (2001), 'Superplastic deformation of ice: experimental observations', *J. Geophys. Res.* **106**(M6), 11017–11030.
Halfar, P. (1981), 'On the dynamics of the ice sheets', *J. Geophys. Res.* **86**(C11), 11065–1102.
Halfar, P. (1983), 'On the dynamics of the ice sheets 2', *J. Geophys. Res.* **88**(C10), 6043–6051.
Hindmarsh, R. C. A. (1990), 'Time–scales and degrees of freedom operating in the evolution of continental ice sheets', *Trans. R. Soc. Edinburgh, Ser. Earth Sci.* **81**(4), 371–384.
Hindmarsh, R. C. A. & Payne, A. J. (1996), 'Time–step limits for stable solutions of the ice–sheet equation', *Ann. Glaciol.* **23**, 74–85.
Hutter, K. (1983), *Theoretical Glaciology*, D. Reidel.
Huybrechts, P. et al. (1996), 'The EISMINT benchmarks for testing ice-sheet models', *Ann. Glaciol.* **23**, 1–12.
Mahaffy, M. W. (1976), 'A three–dimensional numerical model of ice sheets: tests on the Barnes Ice Cap, Northwest Territories', *J. Geophys. Res.* **81**(6), 1059–1066.
Morton, K. W. & Mayers, D. F. (1994), *Numerical Solutions of Partial Differential Equations: An Introduction*, Cambridge University Press.
Nye, J. F. (1957), 'The distribution of stress and velocity in glaciers and ice-sheets', *Proc. Royal Soc. London A* **239**, 113–133.
Nye, J. F. (2000), 'A flow model for the polar caps of Mars', *J. Glaciol.* **46**(154), 438–444.
Paterson, W. S. B. (1994), *The Physics of Glaciers*, 3rd edn, Pergamon.
Payne, A. et al. (2000), 'Results from the EISMINT model intercomparison: the effects of thermomechanical coupling', *J. Glaciol.* **153**, 227–238.
Press, W. H., Teukolsky, S. A., Vetterling, W. T. & Flannery, B. P. (1992), *Numerical Recipes in Fortran: The Art of Scientific Computing*, 2nd edn, Cambridge University Press.
van der Veen, C. J. (1999), *Fundamentals of Glacier Dynamics*, Balkema.

Appendix: Implementation of Crank-Nicolson with Newton iteration

In the interest of reproducibility, we briefly describe the Crank-Nicolson (Mahaffy 1976, Morton & Mayers 1994) method used in the applications section. First, equation (21) is equivalent to a nonlinear system $F(h) = b$ for unknown values $h = \{h_{l+1,j}\}$. More specifically, the system is $F_j(h) = b_j$, with unknowns $h_j = h_{l+1,j}$, for fixed $l+1$ and $j = -(N/2)+1, \ldots, (N/2)-1$. We define $R = \Delta t/(2\Delta x)$ and

$$Q(a|b) = -\frac{\Gamma}{n+2}\left(\frac{a+b}{2}\right)^{n+2}\left(\frac{a-b}{\Delta x}\right)^{n},$$

at least for n odd. Then

(23)
$$F_j(h) = h_j + RQ(h_{j+1}|h_j) - RQ(h_j|h_{j-1}), \quad b_j = h_{l,j} - RQ(h_{l,j+1}|h_{l,j}) + RQ(h_{l,j}|h_{l,j-1}).$$

Also note $h_{l+1,\pm N/2} = 0$ is the (boundary) condition at the limit of the grid.

We solve this nonlinear system by Newton-Raphson iteration (Press, Teukolsky, Vetterling & Flannery 1992), that is, iterated linearization. One can describe the iteration this way: Let $h^{(s)}$ be an approximation to the values $h_{l+1,j}$ for $j = -(N/2)+1, \ldots, (N/2)-$

1, and suppose $h^{(s+1)}$ is the next approximation in the iteration. The linearization of $F(h) = b$ is the matrix problem

$$J(h^{(s)})\Delta h = b - F(h^{(s)}) \tag{24}$$

where $\Delta h = h^{(s+1)} - h^{(s)}$ and $J(h)$ is the Jacobian of $F(h)$. Note that if $h^{(s)}$ is known and we solve (24) for Δh then $h^{(s+1)} = h^{(s)} + \Delta h$ is an easy update.

The Jacobian is easy to describe. Denote the partial derivatives of $Q(a|b)$ by $Q_1(a|b)$ and $Q_2(a|b)$, respectively. Then

$$J(h)_{jk} = \frac{\partial F_j(h)}{\partial h_k} = \begin{cases} 1 - RQ_2(h_{j+1}|h_j) + RQ_1(h_j|h_{j-1}), & k = j, \\ -RQ_1(h_{j+1}|h_j), & k = j+1, \\ RQ_2(h_j|h_{j-1}), & k = j-1, \\ 0, & \text{otherwise}, \end{cases}$$

an $(N-1) \times (N-1)$ tridiagonal matrix. Of course, in two horizontal dimensions $J(h)$ is a matrix with nontrivial sparse structure. In that case we might do ADI (Morton & Mayers 1994).

In validating Crank-Nicolson as described in the main text, we use $h_j^{(0)}$ as the result of an explicit type I step and then compute $h_j^{(4)}$ as our final step. That is, we use a fixed number (four) of Newton iterations after using the explicit step as a good first guess.

Dept. of Mathematical Sciences, University of Alaska, Fairbanks AK 99775
E-mail address: ffelb@uaf.edu

Geophysical Institute, University of Alaska, Fairbanks AK 99775

Dept. of Mathematical Sciences, University of Alaska, Fairbanks AK 99775

Dept. of Mathematical Sciences, University of Alaska, Fairbanks AK 99775

Geophysical Institute, University of Alaska, Fairbanks AK 99775